Rare Metal Materials and Engineering
Volume 48, Issue 9, September 2019
Available online at www.rmme.ac.cn

Science Press

Cite this article as: Rare Metal Materials and Engineering, 2019, 48(9): 2815-2820.

ARTICLE

Gas Sensing Properties of Graphene-$ZnGa_2O_4$ Composites Prepared by Hydrothermal Method

Li Xue[1], Zhang Jun[1], Chu Xiangfeng[1], Liang Shiming[2], Bai Linshan[1], Dong Yongping[1]

[1]Anhui University of Technology, Maanshan 243002, China; [2] Linyi University, Linyi 276000, China

Abstract: A series of graphene-$ZnGa_2O_4$ composites (G-$ZnGa_2O_4$) were synthesized by a hydrothermal method. The prepared samples were characterized by XRD, SEM, TEM, Raman and XPS. The gas sensing properties of the G-$ZnGa_2O_4$ composites were investigated. The results indicate that the graphene content has a great influence on the response and the gas sensing selectivity; the optimal composition of G-$ZnGa_2O_4$ gas sensing composites is 0.1wt% G-$ZnGa_2O_4$. The sensor based on 0.1wt% G-$ZnGa_2O_4$ exhibits high response to 1000 μL/L formaldehyde when operated at 203 °C and the response reaches 32.2; the detection limit for formaldehyde is as low as 1 μL/L; the gas sensing selectivity to formaldehyde is also good and the ratio of $S_{1000\ \mu L/L\ formaldehyde}$ and $S_{1000\ \mu L/L\ acetone}$ reaches 26.8. The response time and recovery time for 1000 μL/L formaldehyde are 11 and 5 s and the response time and recovery time for 1 μL/L formaldehyde are 6 and 5 s, respectively.

Key words: graphene; $ZnGa_2O_4$; formaldehyde; gas sensor

In the past several decades, many researchers showed great interest in semiconductor gas sensors for detecting gases in the environment, owing to the increasing release of harmful gases from industrial process and industrial products. It has been reported that the toxic air pollutants such as CO[1], NO_x[2], NH_3[3,4], LPG[5], HCHO[6], benzene[7], toluene[8], trimethylamine[9,10] and acetone[11, 12], might be detected using metal oxide gas sensors. Spinel complex oxides, including $ZnFe_2O_4$[13-16], $NiFe_2O_4$[14, 17-19], $CuGa_2O_4$[20, 21] and $ZnGa_2O_4$ [22, 23], were widely reported as gas sensing materials. $ZnGa_2O_4$ nano-material prepared by high-energy ball milling method exhibited high responses to NO_2 at 240 °C and to LPG, ethanol, H_2 and CO at 340 °C.

Graphene could change the gas sensing response and gas sensing selectivity of metal oxides. The responses of SnO_2/reduced graphene oxide (RGO) nanocomposites towards NO_2 and the optimal operating temperature were dependent on the ratio of SnO_2/RGO[24, 25]. The sensor based on the nanocomposite of a few layer graphene/SnO_2 prepared by ultrasound-assisted synthesis showed high response to LPG at room temperature and the operating temperature could be drastically decreased in contrast to pure SnO_2 sensor[26]. Inclusion of graphene into ZnO greatly reduced the optimal operating temperature and increased the gas sensing response of graphene/ZnO composite to hydrogen[27]. ZnO-RGO composites synthesized by a solvothermal method had preferential detection of C_2H_2, good selectivity, long-term stability and fast response/recovery time when operating at 250 °C[28], which demonstrated that graphene addition would be effective in improving the C_2H_2 sensing performance of ZnO-based sensors. The response to ethanol of ZnO/graphene composite composed of cocoon-like ZnO nanoparticles and graphene sheets was nearly 5 times higher than that of pure ZnO[29]; the sensor based on the In_2O_3-RGO nanocomposites exhibited excellent selectivity, high response, and relatively short response and recovery time for detection of NO_2 at room temperature and the excellent sensing properties resulted from the composition and structure advantages of the In_2O_3-RGO nanocomposites[30]. In comparison with pristine rGO sensor, the MoO_3-RGO chemiresistors have a clear response to hy-

Received date: September 09, 2018
Corresponding author: Chu Xiangfeng, Ph. D., School of Chemistry and Chemical Engineering, Anhui University of Technology, Maanshan 243002, P. R. China, E-mail: maschem@sohu.com

Copyright © 2019, Northwest Institute for Nonferrous Metal Research. Published by Science Press. All rights reserved.

drogen sulfide down to 50 μL/L at 70 °C[31]. Graphene-TiO_2 nanocomposite layers prepared by using a sol-gel method along with spin coating deposition showed higher response toward sensing CO_2 compared with pristine TiO_2 sensors at optimum temperature[32]. Even for the same kind of metal oxide/graphene composite materials, different preparation methods led to different microstructure, which resulted in different gas sensitivity, different optimal operating temperature and different gas sensing selectivity.

In this research, pure $ZnGa_2O_4$ nano-material and graphene/$ZnGa_2O_4$ nano-composites were prepared and the gas sensing properties of the materials were also investigated. It was found that the sensor based on 0.1% G-$ZnGa_2O_4$ exhibited high response and gas sensing selectivity to formaldehyde when operated at 203 °C.

1 Experiment

All the chemicals used in these experiments were analytical pure reagents (Shanghai Chemical Reagent Company). The graphene was single-layer graphene (Suzhou Heng Qiu Graphene Technology Co., Ltd.).

Ga_2O_3 was added into the mixture solution of concentrated nitric acid and concentrated hydrochloric acid. Ga_2O_3 was dissolved after refluxing the mixture at 90 °C for 4 h. The graphene was dispersed in de-ionized water by sonicating for 30 min, Ga^{3+} solution and $ZnSO_4$ solution were added to the graphene suspension, and the mixed solution was stirred for 2 h; the molar ratio of n_{Zn}:n_{Ga} = 1:2, and the mass fraction (wt%) of graphene to $ZnGa_2O_4$ were 0.00, 0.05, 0.10, 0.25, 0.50 and 1.0 and the obtained corresponding samples were labeled as pure $ZnGa_2O_4$, S-1, S-2, S-3, S-4 and S-5, respectively. 2.0 mol/L NaOH was added to the above solution until the pH was 13.50. Then the mixture was transferred into a 50 mL autoclave and kept at 170 °C for 12 h. Finally, the product was washed with deionized water and ethanol for 6~8 times and dried at 80 °C for 12 h in an oven.

The crystallographic structure of the products was investigated by X-ray diffraction (XRD, Bruker D8 Advance, λ =0.154 056 nm, 40 kV, 40 mA, the scanning rate of 2°/min and the scanning range of 10°~80°). The morphologies and microstructure of the materials were observed by scanning electron microscopy (SEM, Hitachi S-4800; 10 kV) and transmission electron microscope (TEM, JEM 1200EX; 120 kV). Raman spectra analyses were performed with a Renishaw Invia spectrometer with a 532 nm wavelength laser in range of 3200~100 cm^{-1}. The specific surface areas and the pore size were obtained through N_2 adsorption-desorption isotherms (APAP2010MC). The chemical composition of surface was analyzed by X-ray Photoelectron Spectroscopy (XPS, ESCALAB250Xi) with all of the binding energy corrected by contaminant carbon (C 1s = 284.6 eV).

The method of sensor device fabrication and gas sensing property measurement were reported in our previous work[33]. The response (S=R_a/R_g) of the sensor was defined as the ratio of the stable electrical resistance of the sensor in air (R_a) to that in the gas mixture of a targeted gas and air (R_g). The response time and recovery time were defined as the time taken by the sensor to achieve 90% value of the final signal[34], respectively.

2 Results and Discussion

Fig.1 shows the XRD patterns of a series of G-$ZnGa_2O_4$ composites with different graphene contents. The main diffraction peaks in the XRD patterns of all samples were consistent with the standard XRD spectrum of $ZnGa_2O_4$ with the face-centered cubic crystal structure (JCPDS no. 38-1240); the diffraction peaks of Ga_2O_3 appeared in the XRD patterns when the contents of graphene were higher than 0.5 wt%; when Ga^{3+} solution and $ZnSO_4$ solution were added to the graphene suspension solution, the functional groups (such as -COOH and -OH) on G sheets captured the metal ions (Zn^{2+} and Ga^{3+}) efficiently due to a strong electrostatic effect[35], -OH and –COOH caused the nucleation and in-situ growth of Zn-Ga precursor [$Zn(OH)_2$ and $Ga(OH)_3$] on graphene substrate, and the resulting Zn-Ga precursor anchored on G substrate would form $ZnGa_2O_4$ in the process of hydrothermal reaction; The valence state of Ga^{3+} was higher than that of Zn^{2+}, which led to more Ga^{3+} being adsorbed on the surface of graphene than Zn^{2+}, the excess Ga^{3+} on the surface of graphene formed $Ga(OH)_3$, $Ga(OH)_3$ decomposed into Ga_2O_3 and H_2O; the excess Zn^{2+} in the solution did not form $ZnGa_2O_4$ and existed in the form of ZnO_2^{2-} after the hydrothermal reaction stopped, and ZnO_2^{2-} ions were moved in the process of washing; with the increase of graphene content, the amounts of the excess Ga^{3+} on the surface of graphene and excessive Zn^{2+} in the solution increased, which could explain the reason that the diffraction peaks of Ga_2O_3 appeared in XRD patterns when the contents of graphene were higher than 0.5 wt%. Graphene had influenced the nucleation and in-situ growth of complex metal oxides, which was also reported in Ref.[36, 37]. The diffraction peaks of graphene could not be seen in the XRD patterns of the G-$ZnGa_2O_4$ composites, which resulted from the low diffraction intensity and shielding of the graphene peaks by those of $ZnGa_2O_4$[38, 39]. The average crystal sizes calculated by Scherrer's formula of $ZnGa_2O_4$ crystals in G-$ZnGa_2O_4$ composites (pure $ZnGa_2O_4$, S-1, S-2, S-3, S-4 and S-5) were 5, 6, 6, 7, 5 and 6 nm, respectively.

Fig.2 shows SEM images of graphene, pure $ZnGa_2O_4$, S-2 and HRTEM image of S-2 samples. It could be clearly observed from Fig.2a that the graphene had a thin layer structure with a large number of folds on the surface; the particle sizes of pure $ZnGa_2O_4$ were in the range of 50~150 nm shown in Fig.2b, and the SEM results were in contradiction with the data of XRD , which implied that the big particles were composed of small crystallites; there were a lot of laminar sheets in S-2, the frameworks of the sheets were graphene sheets, and small $ZnGa_2O_4$ crystals were distributed uniformly on the two sides of graphene sheets；the HRTEM image of S-2

sample was shown in Fig.2d, the plane spacing of 0.289 and 0.253 nm could be ascribed to the lattice fringe of $ZnGa_2O_4$ crystal (220) and (311), respectively[40-42].

X-ray photoelectron spectroscopy (XPS) was adopted to characterize the composition and chemical state of the elements in G-$ZnGa_2O_4$ composite (S-1). As seen in Fig.3a, S-1 was composed of Zn, Ga, O and C obviously; The C1s peak in Fig.3b was asymmetrical and could be disassembled into three peaks located at 284.5, 285.2 and 288.9 eV, corresponding to graphitic carbon in graphene, carbon in C-O and carbon in O-C-O, respectively; the carbon atoms in different oxygen-containing functional groups might be originated from the residual oxygen-containing functional groups on graphene and the reconstructed oxygen-containing bonds between C atoms and the surface oxygen of $ZnGa_2O_4$[43, 44], and this analysis on XPS peaks of C 1s proved that graphene existed in S-1. The peak of Ga3d was located at 20.0 eV, which accorded with the result reported in Ref.[45]. There were two peaks located at 1021.7 and 1044.7 eV which could be assigned to Zn $2p_{3/2}$ and Zn $2p_{1/2}$, respectively[35, 46]. A high-resolution peak of O 1s spectrum in Fig.3e could be resolved to two peaks with the energy of 530.43 eV for lattice oxygen and 531.33 eV for surface adsorbed oxygen species, and the surface absorbed oxygen species had an significant influence on the gas sensing properties of materials[35]. Fig.3f displays the Raman spectra of S-2 and graphene. It could be observed that there were two sharp and strong absorption peaks at 1324 and 1593 cm^{-1}, which accorded with the characteristic peaks D and G of graphene, respectively. The peak D represented the edge defects of graphene which was related to the destruction of sp^2 hybridized carbon atoms and the formation of sp^3 hybridized carbon atoms; while the peak G correlated to the vibration of the sp^2 hybridized carbon atoms existing in the two-dimensional hexagonal lattice of graphene, G peak represented the E_{2g} vibrational mode of the sp^2 hybridized carbon atoms[43]. The appearance of peak D and peak G in the Raman spectrum of S-2 sample indicated that graphene had been successfully doped into $ZnGa_2O_4$.

Fig.4 depicts the responses of pure $ZnGa_2O_4$ and G-$ZnGa_2O_4$ composites to 1000 μL/L formaldehyde at different operating temperatures. The responses of pure $ZnGa_2O_4$ to 1000 μL/L formaldehyde were very low, the maximum values appeared at 203 and 246 which were only 4.0; the responses of G-$ZnGa_2O_4$ composites reached maximum values when operating at 203 °C; the graphene content of G-$ZnGa_2O_4$ composites had a significant effect on the maximum gas re-

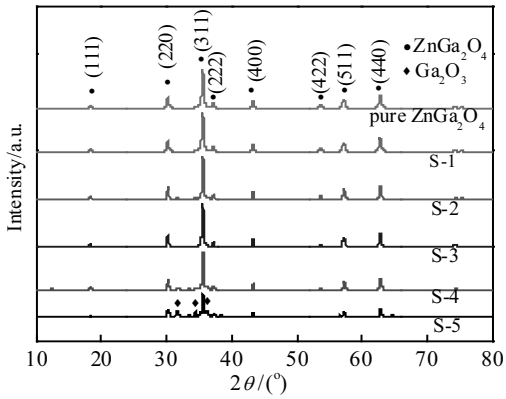

Fig.1 XRD patterns of pure $ZnGa_2O_4$, 0.05% G-$ZnGa_2O_4$ (S-1), 0.1% G-$ZnGa_2O_4$ (S-2), 0.25% G-$ZnGa_2O_4$ (S-3), 0.5% G-$ZnGa_2O_4$ (S-4), and 1% G-$ZnGa_2O_4$ (S-5)

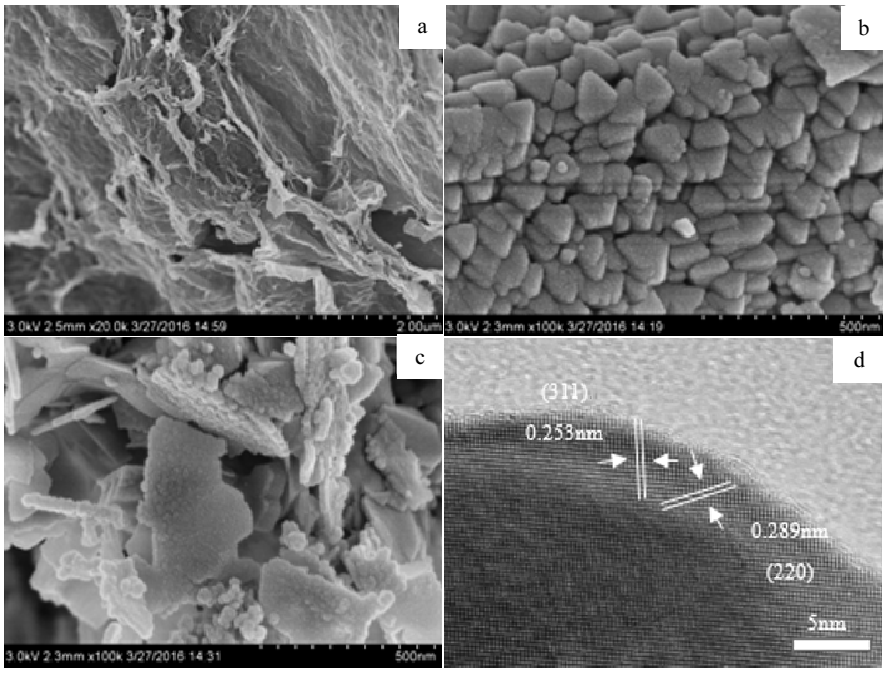

Fig.2 SEM images of graphene (a), pure $ZnGa_2O_4$ (b), S-2 (c), and the HRTEM image of S-2 (d)

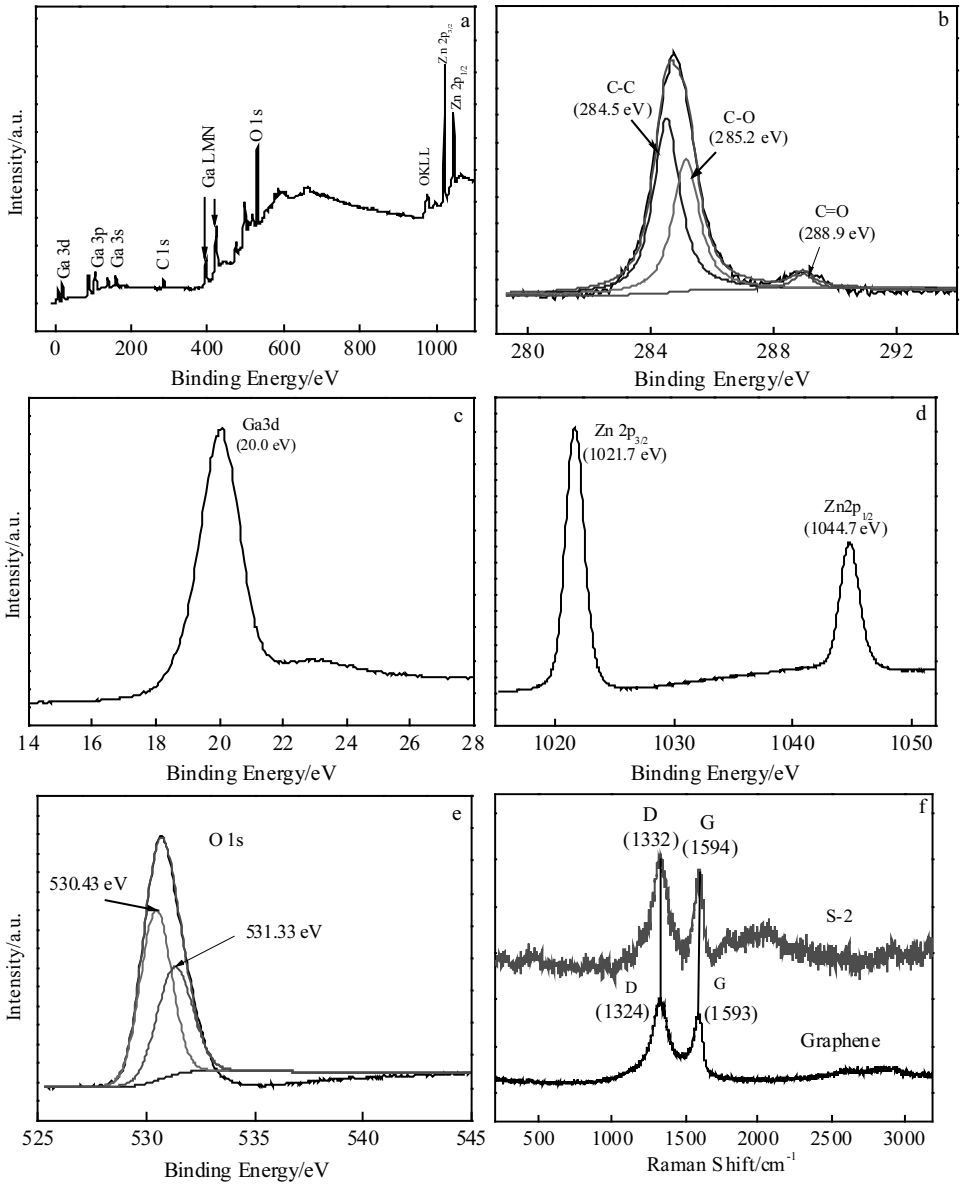

Fig.3 XPS spectra of S-1 composite: (a) survey spectrum, (b, c, d, e) high-resolution spectra for C 1s, Ga 3d, Zn 2p, O 1s peaks, respectively, and (f) Raman spectra of S-2 and graphene

sponse of the materials; when the graphene content was lower than 0.1 wt%, the maximum response increased with the graphene content increasing; on the contrary, the maximum response decreased when the graphene content was higher than 0.1 wt%. The sensor based on S-2 (0.1 wt% G-$ZnGa_2O_4$ composite) exhibited high response to 1000 μL/L formaldehyde, and the response was 32.2. The maximum response value could be obtained at a particular G/$ZnGa_2O_4$ ratio, and this phenomenon was also reported in literature [24]. Graphene was p-type semiconductor and $ZnGa_2O_4$ was n-type semiconductor; doping graphene resulted in formation of an n-p heterojunction at $ZnGa_2O_4$-graphene interface, which was propitious to gas sensing; the "shortcut" between graphene and graphene would increase if the graphene content increased, which was not advantageous to gas sensing[24].

Fig.5 shows the response of sensor based on S-2 to six kinds of gases (1000 μL/L) at different operating temperatures. It could be seen that S-2 exhibited high response and gas sensing selectivity to 1000 μL/L formaldehyde when operating at 203 °C, and the responses were 32.2; while the responses to other kinds of gases were no higher than 2.5, and the ratio of $S_{1000\ \mu L/L\ formaldehyde}$ and $S_{1000\ \mu L/L\ acetone}$ reached 26.8. But when operating at room temperature, the sensor based on S-2 showed good gas sensing selectivity to ammonia, the re-

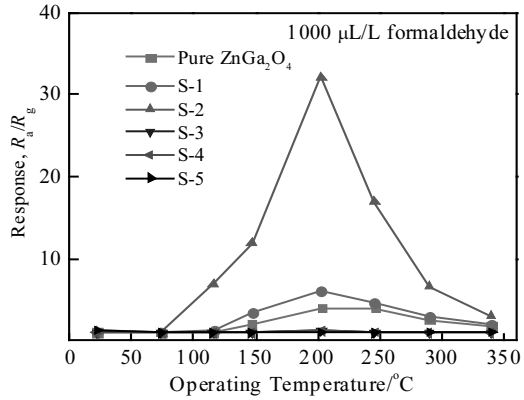

Fig.4 Responses of pure $ZnGa_2O_4$ and G-$ZnGa_2O_4$ composites to 1000 μL/L formaldehyde at different operating temperatures

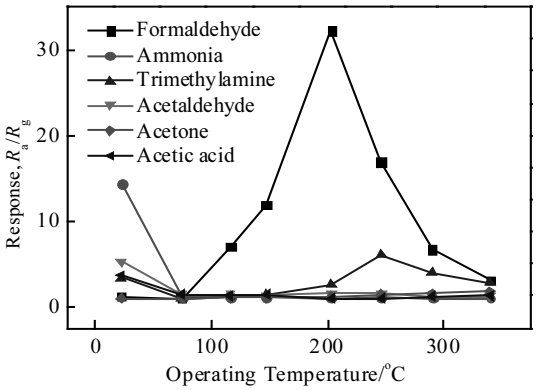

Fig.5 Response of sensor based on S-2 to six kinds of gases (1000 μL/L) at different operating temperatures

sponse to 1000 μL/L ammonia reached 14.4, and the responses to other kinds of gases were lower than 5.3. The formaldehyde sensing mechanism of metal oxides and graphene/metals oxide composites have been investigated by many researchers[47, 48], The adsorbed oxygen on the surface of $ZnGa_2O_4$ captured the electrons from the conduction band of $ZnGa_2O_4$ in air, which resulted in the electrical resistance increase of $ZnGa_2O_4$ sensor device; when the sensor device was placed in formaldehyde atmosphere, HCHO molecules reacted with the adsorbed oxygen, the electrons captured by the adsorbed oxygen were released to the conduction band, which led to the electrical resistance decrease of the sensor device; the reaction occurred on the surface of $ZnGa_2O_4$ was following:

$$HCHO_{(ads)} + 2O^-_{(ads)} \rightarrow CO_2 + H_2O + 2e^-$$

Fig.6 shows the response/recovery characteristics of the S-2 sensor to different concentrations of HCHO when operating at 203 °C; the response/recovery times for 1000, 500, 250, 100, 50, 10 and 1 μL/L HCHO were 16s/16.5s, 10s/4s, 5s/17s, 25s/11s, 9s /12s, 9s/20s and 5s/5s, respectively; the response

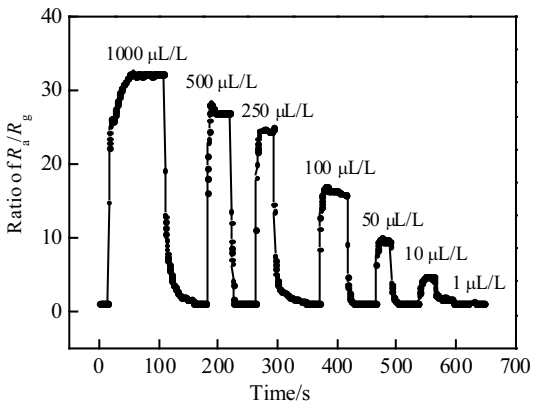

Fig.6 Response/recovery characteristics of the S-2 sensor to different concentrations of HCHO when operating at 203 °C

to 1 μL/L was 1.2, which manifested that the detection limit for formaldehyde reached 1 μL/L.

3 Conclusions

1) Graphene-$ZnGa_2O_4$ composites are synthesized by hydrothermal method.

2) The graphene content has a great influence on the response and the gas sensing selectivity, and the optimal composition of G-$ZnGa_2O_4$ gas sensing material is 0.1wt% G-$ZnGa_2O_4$.

3) The sensor based on 0.1wt% G-$ZnGa_2O_4$ exhibits high response to 1000 μL/L formaldehyde when operated at 203 °C, the detection limit for formaldehyde is as low as 1 μL/L; the gas sensing selectivity to formaldehyde is also good, and the ratio of $S_{1000\ \mu L/L\ formaldehyde}$ and $S_{1000\ \mu L/L\ acetone}$ reaches 26.8. The response time and recovery time for 1 μL/L formaldehyde are 6 and 5 s, respectively.

References

1 Wang L, Zhang R, Zhou T *et al*. *Sensors & Actuators B Chemical* [J], 2017, 239: 211

2 Mane A A, Moholkar A V. *Applied Surface Science* [J], 2017, 405: 427

3 Wang Y, Liu J, Cui X *et al*. *Sensors & Actuators B Chemical* [J], 2017, 238: 473

4 Bedi R K, Singh I. *Acs Appl Mater Interfaces* [J], 2010, 2(5): 1361

5 Vijayanand S, Joy P A, Potdar H S *et al*. *Sensors & Actuators B Chemical* [J], 2011, 152(1): 121

6 Tang W, Wang J, Yao P *et al*. *Journal of Materials Science*[J], 2014, 49(3): 1246

7 Ghaddab B, Berger F, Sanchez J B *et al*. *Sensors & Actuators B Chemical*[J], 2011, 152(1): 68

8 Liu L, Zhang Y, Wang G *et al*. *Sensors & Actuators B Chemical* [J], 2011, 160(1): 448

9 Lee C S, Kim I D, Lee J H. *Sensors & Actuators B Chemical*[J], 2013, 181(5): 463
10 Pandeeswari R, Jeyaprakash B G. *Biosensors & Bioelectronics* [J], 2014, 53: 182
11 Xing R, Sheng K, Xu L *et al*. *Rsc Advances*[J], 2016, 6: 57 389
12 Al-Hadeethi Y, Umar A, Ibrahim A A *et al*. *Ceramics International*[J], 2017, 43(9): 6765
13 Zhou X, Wang B, Sun H *et al*. *Nanoscale*[J], 2015, 8(10): 5446
14 Xu Y, Sun D, Hao H *et al*. *Rsc Advances*[J], 2016, 6(101): 98 994
15 Wang Y, Liu F, Yang Q *et al*. *Materials Letters*[J], 2016, 183: 378
16 Sahoo R, Santra S, Ray C *et al*. *New Journal of Chemistry*[J], 2016, 40: 1861
17 Satyanarayana L, Reddy K M, Manorama S V. *Materials Chemistry and Physics*[J], 2003, 82: 21
18 Patil J Y, Nadargi D Y, Gurav J L *et al*. *Materials Letters*[J], 2014, 124(6): 144
19 Rao P, Godbole R V, Bhagwat S. *Journal of Magnetism & Magnetic Materials*[J], 2016, 416: 292
20 Biswas S K, Sarkar A, Pathak A *et al*. *Talanta*[J], 2010, 81(4-5): 1607
21 Chen H, Li G D, Fan M *et al*. *Sensors & Actuators B Chemical* [J], 2017, 240: 689
22 Chen C, Li G, Liu Y. *Powder Technology*[J], 2015, 281: 7
23 Satyanarayana L, Gopal Reddy C V, Manorama S V *et al*. *Sensors & Actuators B Chemical*[J], 1998, 46(1): 1
24 Neri G, Leonardi S G, Latino M *et al*. *Sensors & Actuators B Chemical*[J], 2013, 179(2): 61
25 Zhang H, Feng J, Fei T *et al*. *Sensors & Actuators B Chemical* [J], 2014, 190(1): 472
26 Goutham S, Bykkam S, Sadasivuni K K *et al*. *Microchimica Acta* [J], 2018, 185(1): 69
27 Anand K, Singh O, Singh M P *et al*. *Sensors & Actuators B Chemical* [J], 2014, 195(195): 409
28 Uddin A S M I, Chung G S. *Sensors & Actuators B Chemical*[J], 2014, 205: 338
29 Liang S, Zhu J, Ding J *et al*. *Applied Surface Science*[J], 2015, 357: 1593
30 Gu F, Nie R, Han D *et al*. *Sensors & Actuators B Chemical*[J], 2015, 219: 94
31 Malekalaie M, Jahangiri M, Rashidi A M *et al*. *Materials Science in Semiconductor Processing*[J], 2015, 38: 93
32 Amiri M T, Ashkarran A A. *Journal of Materials Science Materials in Electronics*[J], 2017, 28(13): 1
33 Hu T, Chu X, Gao F *et al*. *Journal of Solid State Chemistry*[J], 2016, 237: 284
34 Poloju M, Jayababu N, Reddy M V R. *Materials Science and Engineering* [J], 2017, 227: 61
35 Li Z, Xiang Y, Lu S *et al*. *Journal of Alloys & Compounds*[J], 2018, 737: 58
36 Lin J, He J R, Chen Y F *et al*. *Electrochim Acta*[J], 2016, 215: 667
37 Yang S, Wang Q, Miao J *et al*. *Applied Surface Science*[J], 2018, 444: 522
38 Fan Y, Lu H T, Liu J H *et al*. *Colloids & Surfaces B Biointerfaces* [J], 2011, 83(1): 78
39 Liu J, Li S, Zhang B *et al*. *Sensors & Actuators B Chemical*[J], 2017, 249: 715
40 Xua Q, Wu Z C, Hong J H *et al*. *Applied Surface Science*[J], 2015, 353: 419
41 Yang Q, Saeki Y, Izumi S *et al*. *Applied Surface Science*[J], 2010, 256: 6928
42 Chen C, Li G Z, Liu Y L. *Powder Technology*[J], 2015, 281: 7
43 Zhu Y, Li C, Cao C. *RSC Advances*[J], 2013, 3(29): 11 860
44 Wang P, Wang D, Zhang M *et al*. *Sensors & Actuators B Chemical*[J], 2016, 230: 477
45 Thakur V, Shivaprasad S M. *Applied Surface Science*[J], 2015, 327: 389
46 Lu M, Xin O, Wu S *et al*. *Applied Surface Science*[J], 2016, 364: 775
47 Mishra R K, Murali G, Kim T H *et al*. *Rsc Advances*[J], 2017, 7(61): 38 714
48 Rahman M M, Khan S B, Faisal M *et al*. *Sensors & Actuators B Chemical*[J], 2012, S171-172(8): 932

水热法制备石墨烯-镓酸锌复合物及其气敏性能

李　学[1], 张　俊[1], 储向峰[1], 梁士明[2], 白林山[1], 董永平[1]
(1. 安徽工业大学，安徽 马鞍山 243002)
(2. 临沂大学，山东 临沂 276000)

摘　要：通过水热法制备了一系列的石墨烯-镓酸锌复合物。所制备的材料用 XRD，SEM，TEM，拉曼和 XPS 进行表征。同时，探究了复合物的气敏性能。结果表明，石墨烯的含量对复合材料的气敏响应值和选择性有着很大的影响，并且当石墨烯的质量分数在 0.1%时，复合材料的气敏性能最好。当操作温度在 203 ℃时，0.1%石墨烯-镓酸锌复合材料对 1000 μL/L 的甲醛的响应值达 32.2 倍，最低检测限度为 1 μL/L。同时，该材料的选择性也比较优越，对 1000 μL/L 甲醛和 1000 μL/L 丙酮的响应值的比值为 26.8。该材料对 1000 μL/L 甲醛的响应和恢复时间分别为 11 和 5 s，对 1 μL/L 甲醛的响应和恢复时间分别为 6 和 5 s.

关键词：石墨烯；镓酸锌；甲醛；气体传感器

作者简介：李　学，男, 1993 年生，硕士生，安徽工业大学化学与化工学院，安徽 马鞍山 243002, E-mail: 343259560@qq.com